Supporting Information

Angle-Independent Surface-Instability Hydrogel Sensors Enabled by Thickness Control

*Ruoyi Ke[‡], Imri Frenkel[‡], Zixiao Liu, Chuan Wei Zhang, Ping He, Pengju Shi, Abdullatif Jazzar, Yousif Alsaid, Yingjie Du, Sidi Duan, Dong Wu, Mutian Hua, Shuwang Wu, Ximin He**

Department of Materials Science and Engineering, University of California, Los Angeles, CA, 90095, USA

*Corresponding author. Email: ximinhe@ucla.edu

Keywords: hydrogel sensors; surface instability; angle-independent detection; material-based computation; soft robotics

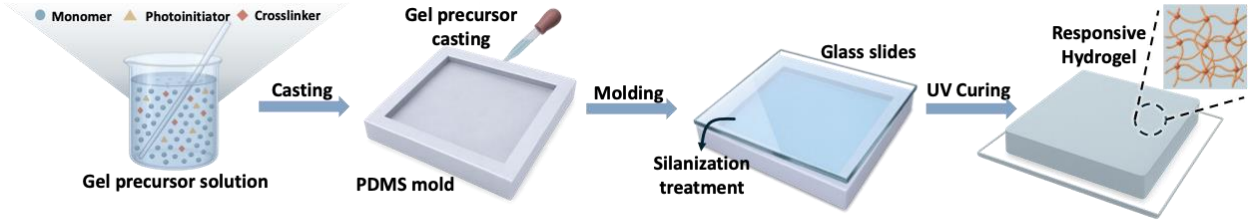

Supplementary Figure S1 Hydrogel sensor fabrication workflow and structural components. Sequential preparation stages from gel precursor solution containing monomer, photoinitiator, and crosslinker components through casting into PDMS molds, molding against functionalized glass slides with silanization treatment, and UV curing polymerization to produce responsive hydrogel films. Glass substrate functionalization enables strong hydrogel adhesion necessary for surface instability formation under swelling-induced stress concentration. Final sensor architecture demonstrates thickness-controlled surface morphology optimization for omnidirectional optical detection capabilities.

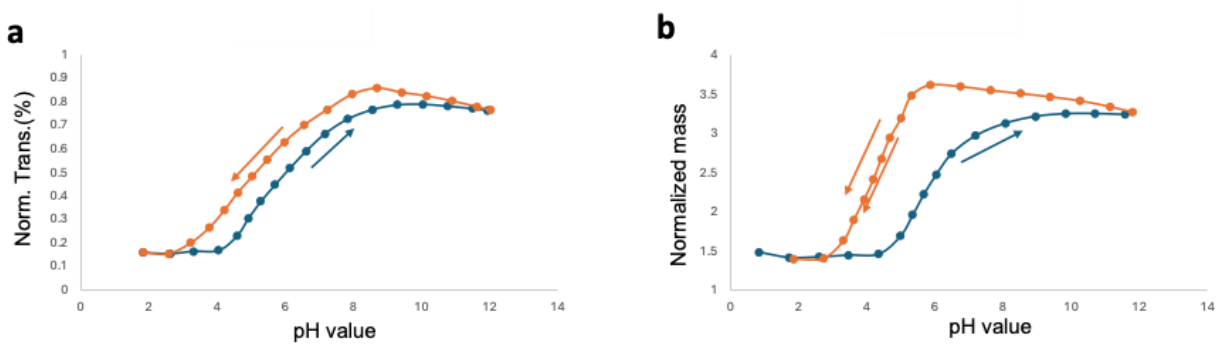

Supplementary Figure S2 Hysteresis characterization of substrate-constrained IIS sensors versus unconstrained hydrogels. (a) Normalized optical transmission at 650 nm during pH cycling (pH 2→12→2) for substrate-constrained PDMAEMA sensors (300 μm thickness, 45% monomer, 3% PEGDA700). (b) Normalized mass-based swelling ratio during identical pH cycling for unconstrained PDMAEMA hydrogels of the same composition.

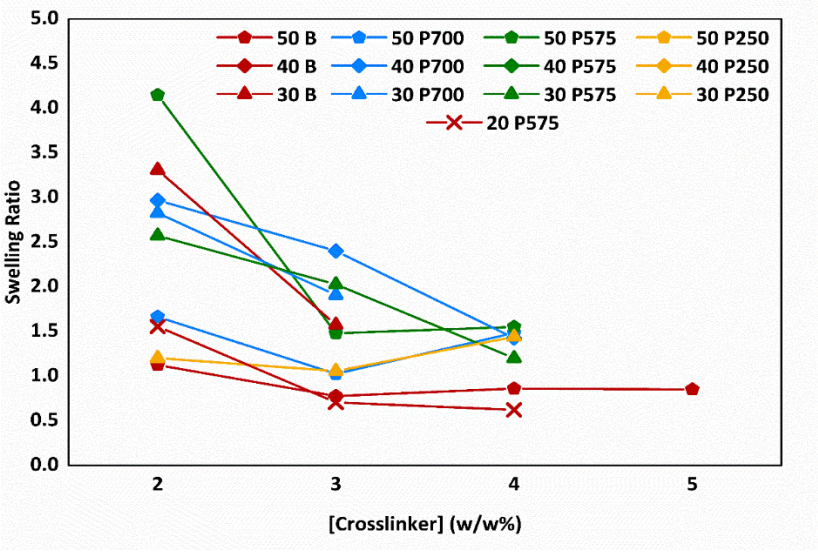

Supplementary Figure S3 Crosslinker vs Swelling Ratio performance. Effect of crosslinker type and monomer content on the swelling of performance of PDMAEMA gels ranging from 20-50% monomer content with 1-5% of either Bis (red), $PEGDA_{700}$ (blue), $PEGDA_{575}$ (green), or $PEGDA_{250}$ (yellow). Increasing crosslink content limited the range of swelling possible as a result of increasing monomer content, however gels with 2% crosslink content or lower polymerize inconsistently or not at all.

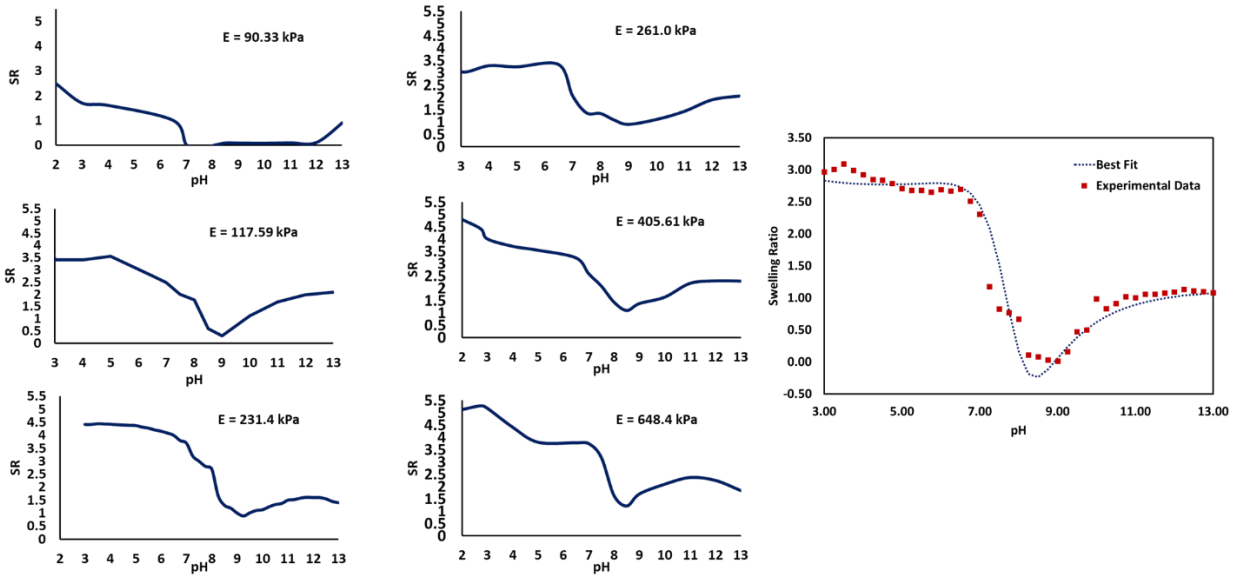

Supplementary Figure S4 Elastic modulus characterization and pH-dependent swelling behavior of PDMAEMA hydrogels. Left and center panels show swelling ratio (SR) as a function of pH for PDMAEMA hydrogels with varying elastic moduli (E = 90.33, 117.59, 231.4, 261.0, 405.61, and 648.4 kPa). All hydrogels exhibit characteristic cationic response with maximum swelling at low pH (~3-4) and minimal swelling at high pH (~9-12). The critical pH transition point shifts to higher values with increasing modulus. Right panel demonstrates the correlation between experimentally measured swelling ratios (red squares) and model predictions (dotted line) across the pH range, showing good agreement particularly in the critical transition region (pH 7-9). The model accurately captures the sharp swelling transition characteristic of volume phase transitions in these systems.

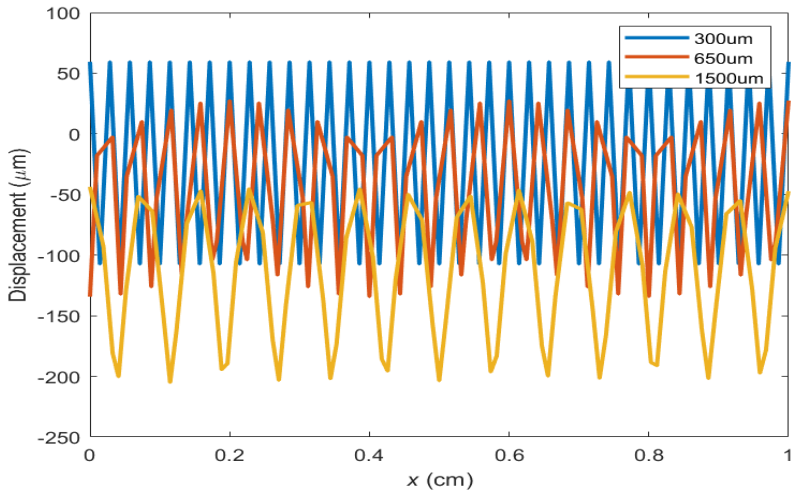

Supplementary Figure S5 COMSOL simulation of thickness-dependent surface displacement profiles. Simulated displacement in the z-direction (perpendicular to film surface) along the x-axis for hydrogel films of different thicknesses (300 μm, 650 μm, and 1500 μm) under identical swelling conditions. The 300 μm film (blue) exhibits high-frequency, low-amplitude wrinkles with wavelengths of approximately 50-100 μm and amplitudes of ~50 μm. The 650 μm film (orange) shows intermediate behavior with wavelengths around 100-150 μm and amplitudes of ~100 μm. The 1500 μm film (yellow) displays low-frequency, high-amplitude undulations with wavelengths exceeding 200 μm and amplitudes reaching ~200 μm. These results confirm the systematic relationship between film thickness and surface instability morphology, where thicker films produce longer wavelength patterns with larger amplitudes.

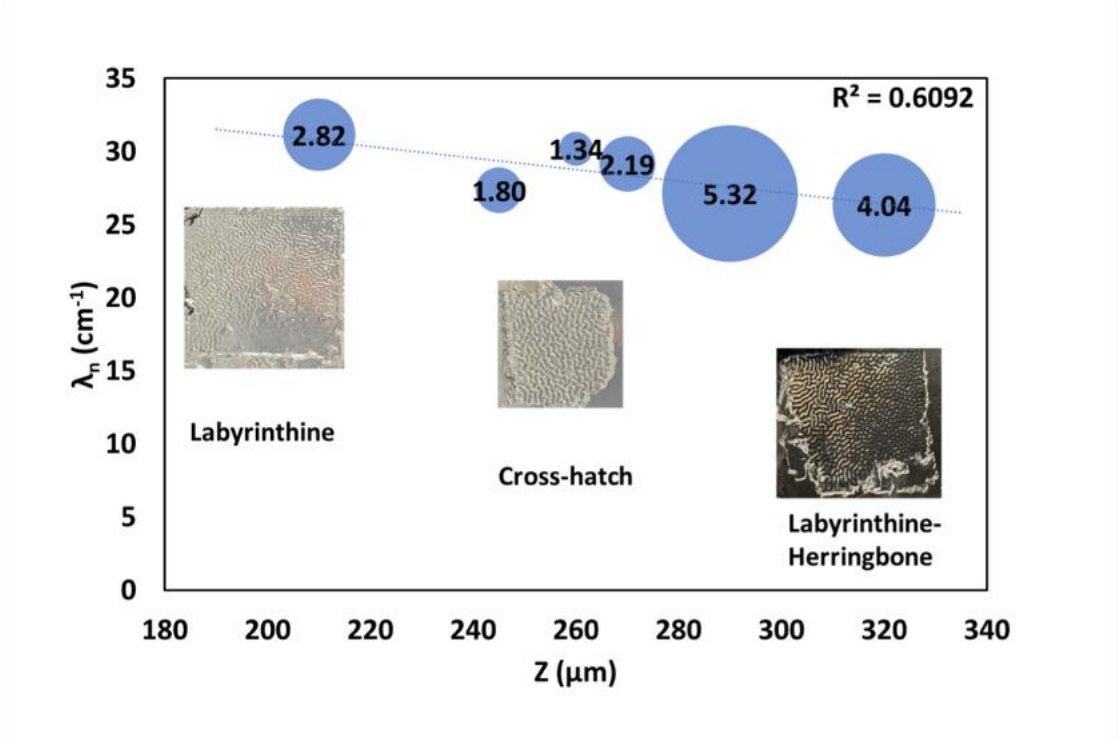

Supplementary Figure S6 Thickness-dependent evolution of wrinkle morphology and wavelength. Plot showing the relationship between film thickness (Z, μm) and wrinkle wavelength (λm, cm^{-1}) for PDMAEMA-based IIS sensors. Data points are sized proportionally to their relative occurrence frequency (indicated by numbers). Three distinct morphological regimes are observed: labyrinthine patterns dominate at lower thicknesses (~210 μm), transitioning through cross-hatch patterns at intermediate thicknesses (~260 μm), to mixed labyrinthine-herringbone patterns at higher thicknesses (~320 μm). Representative optical microscopy images of each morphology type are shown. The decreasing wavelength with increasing thickness ($R^2 = 0.6092$) indicates an inverse relationship between film thickness and wrinkle frequency. Scale bars in microscopy images represent 500 μm.

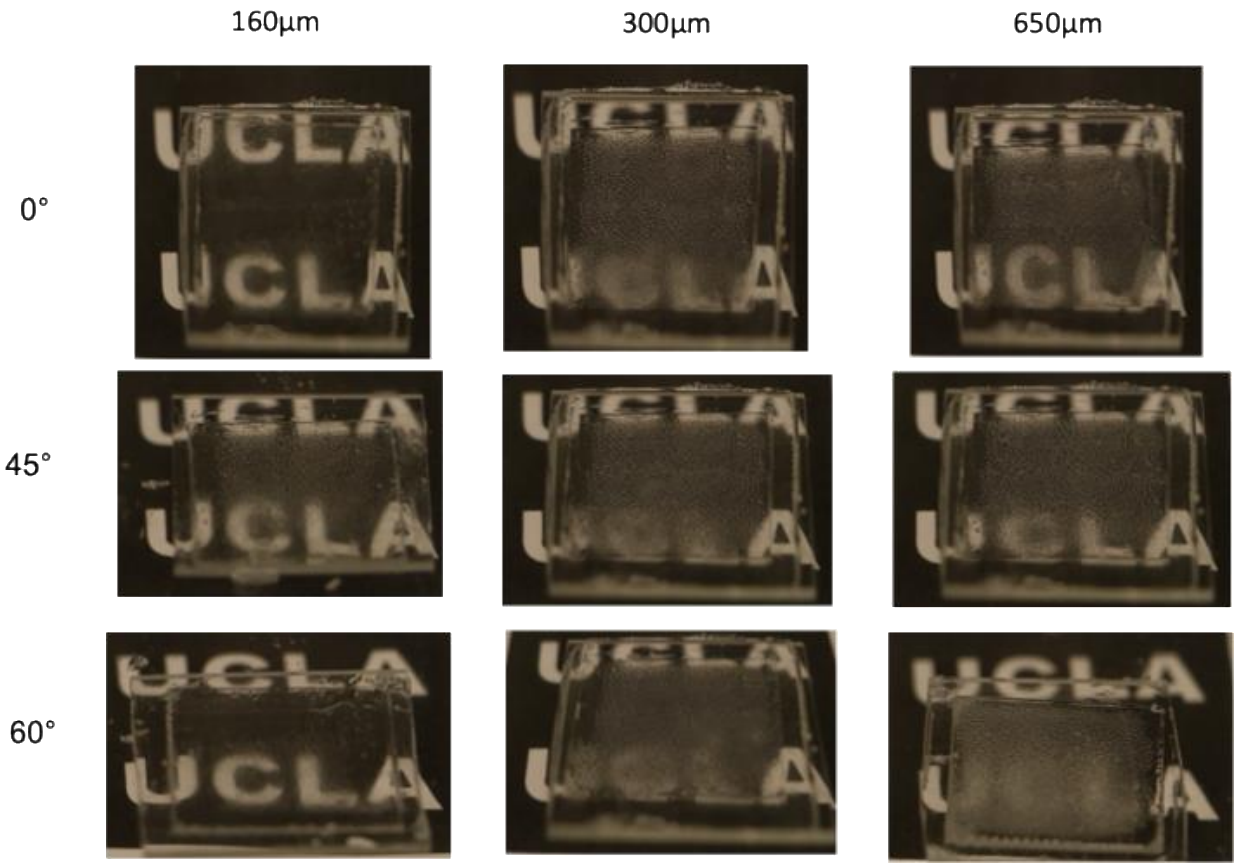

Supplementary Figure S7 Thickness-dependent angular visibility of IIS sensors. Comparison of 160 µm, 300 µm, and 650 µm thick hydrogel films at 0°, 45°, and 60° viewing angles, demonstrating that 300 µm thickness uniquely achieves angle-independent opacity through optimized surface wrinkle dimensions.

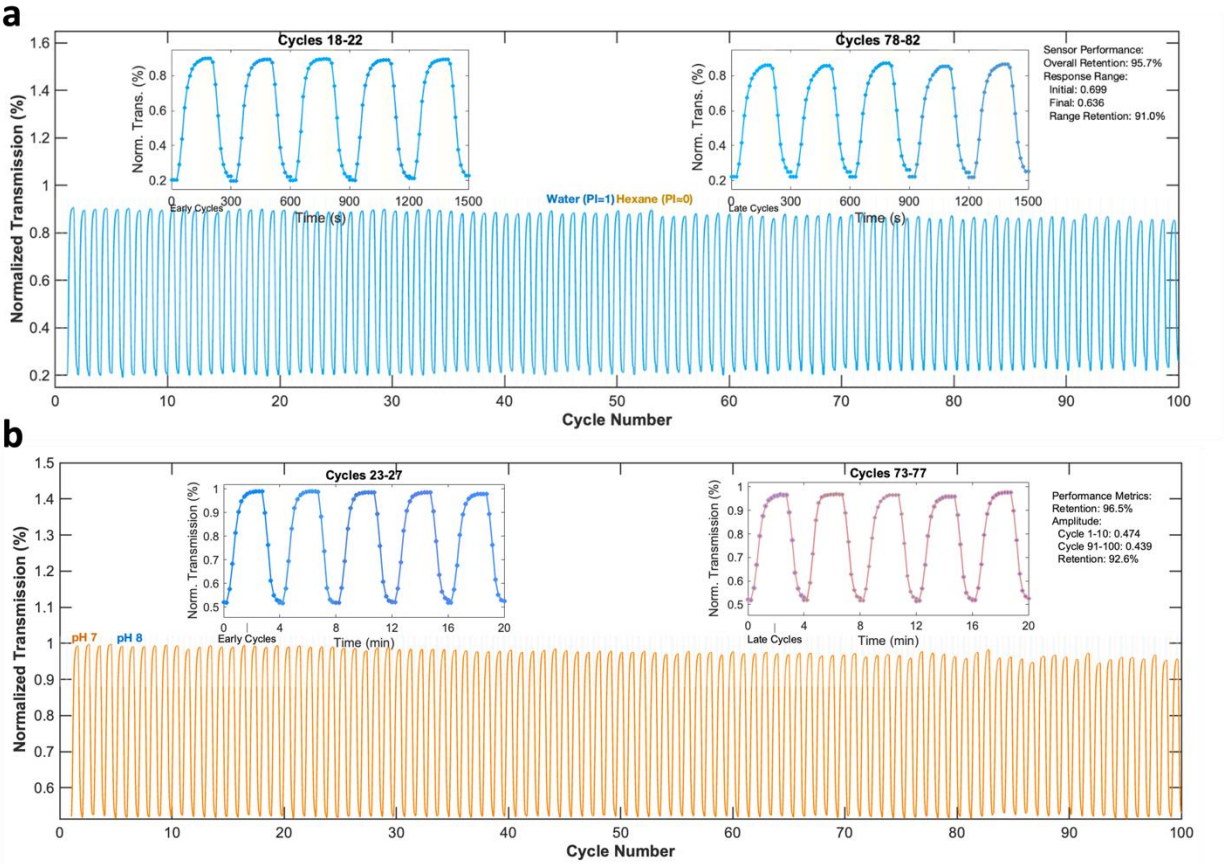

Supplementary Figure S8 Long-term cycling stability of IIS sensors under repeated stimulus switching. (a) Polarity-responsive sensor (P(NIPAm-co-Am), 300 μm thickness) cycling between water (PI = 1, wrinkled state) and hexane (PI ≈ 0, transparent state) over 100 cycles. Sensor maintains switching between 20% and 80% transmission with 91.0% range retention. (b) pH-responsive sensor (PDMAEMA, 45% monomer, 3% PEGDA700, 300 μm thickness) alternating between pH 7 (wrinkled) and pH 8 (transparent) conditions. Consistent switching amplitude between 40% and 90% transmission achieved with 96.5% retention after 100 cycles. Insets show representative early cycles (18-22 and 23-27) and late cycles (78-82 and 73-77) demonstrating minimal performance degradation. Response times remain constant throughout cycling: ~105 seconds for pH transitions and ~120 seconds for polarity transitions. Exceptional durability results from reversible mechanical buckling mechanism without chemical degradation or permanent structural changes.

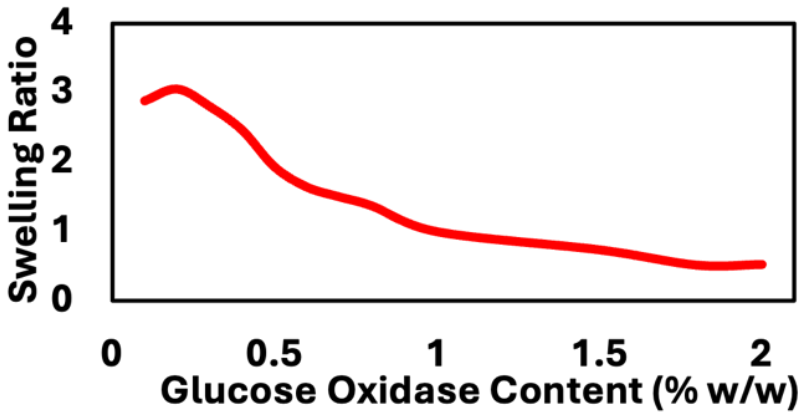

Supplementary Figure S9 Effect of glucose oxidase content on hydrogel swelling behavior. Swelling ratio of PDMAEMA hydrogels as a function of glucose oxidase (GOx) content (0-2% w/w) when exposed to glucose solution. The swelling ratio exhibits a biphasic response: initial increase reaching a maximum of approximately 3.0 at 0.2% w/w GOx loading, followed by a gradual decrease at higher enzyme concentrations. This behavior reflects the dual role of GOx in the network - providing catalytic activity for glucose-responsive swelling at low concentrations while acting as a physical constraint that limits chain extension at higher loadings. The optimal enzyme content for glucose sensing applications lies in the 0.2-0.5% w/w range, balancing sensitivity with mechanical integrity.

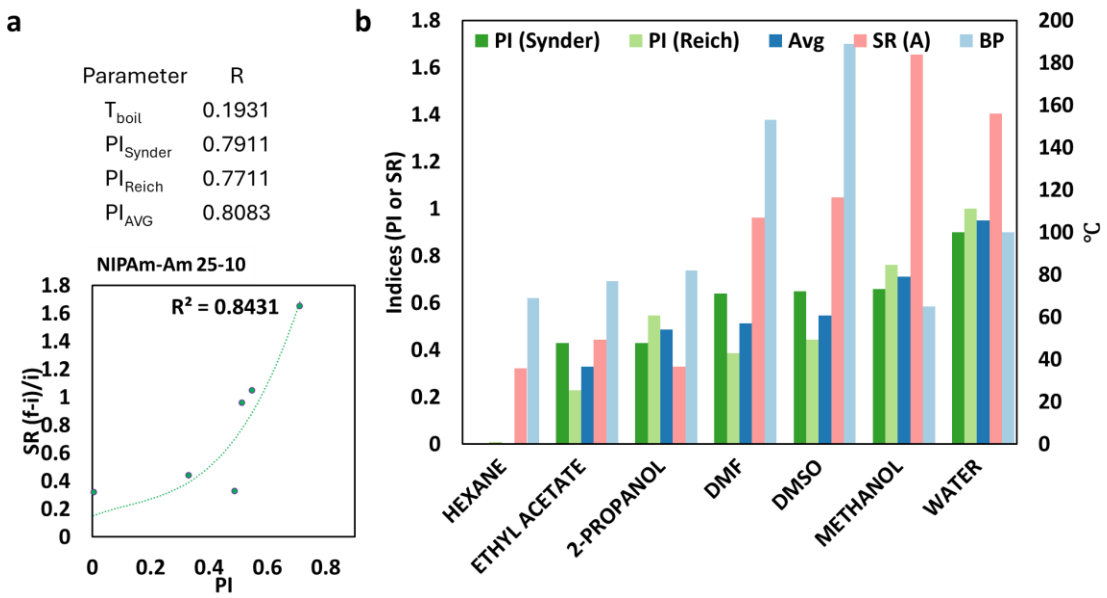

Supplementary Figure S10 (a) Swelling Ratio and correlations of a PI-sensitive gel. (b) Swelling of a NIPam-Am gel in response to organic solvent of various polarity index values.

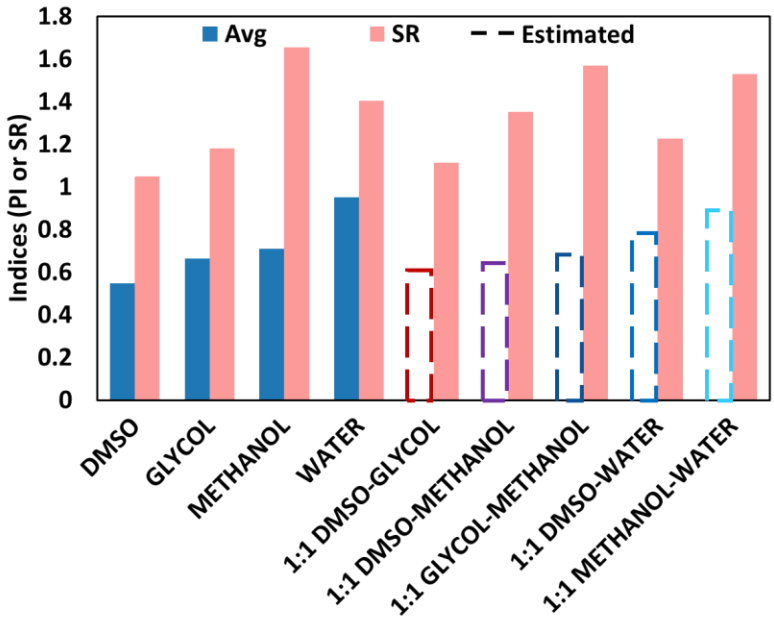

Supplementary Figure S11 Demonstration of PI IISS Application | PI IISS capable of indicating PI of an unknown mixture, critical solvent contamination, or approximate constituent concentrations in a known system.

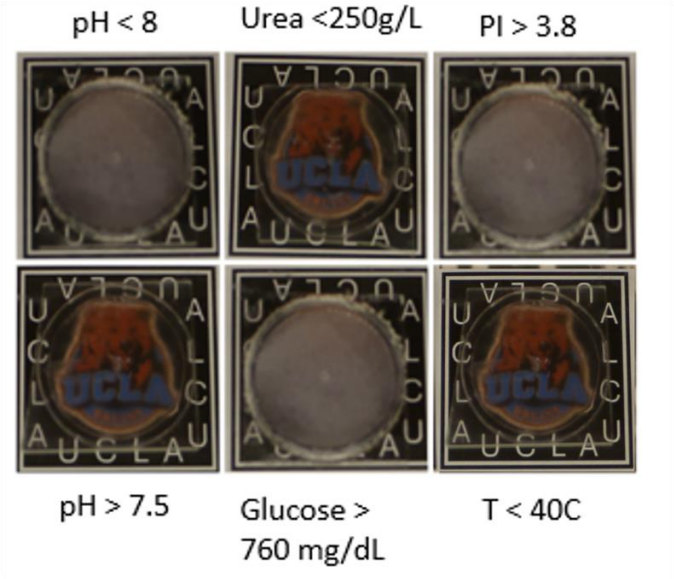

Supplementary Figure S12 Multi-analyte sensing array demonstration. A 2×3 array of IIS sensors with distinct stimulus sensitivities simultaneously monitoring multiple environmental parameters. Each sensor element is designed to respond to specific analytes or conditions: pH < 8 (top left), urea < 250 g/L (top center), polarity index (PI) > 3.8 (top right), pH > 7.5 (bottom left), glucose > 760 mg/dL (bottom center), and temperature < 40°C (bottom right). Under the test conditions shown, three sensors have been activated (appearing opaque/wrinkled with visible UCLA logo distortion): the pH < 8 sensor, pH > 7.5 sensor, and PI > 3.8 sensor, while the urea, glucose, and temperature sensors remain in their transparent state. This visual pattern immediately communicates that the test environment has pH between 7.5 and 8, solvent polarity above 3.8, but contains less than 250 g/L urea and less than 760 mg/dL glucose at temperature below 40°C. The array format demonstrates the capability for multiplexed, equipment-free environmental monitoring through simple visual inspection.

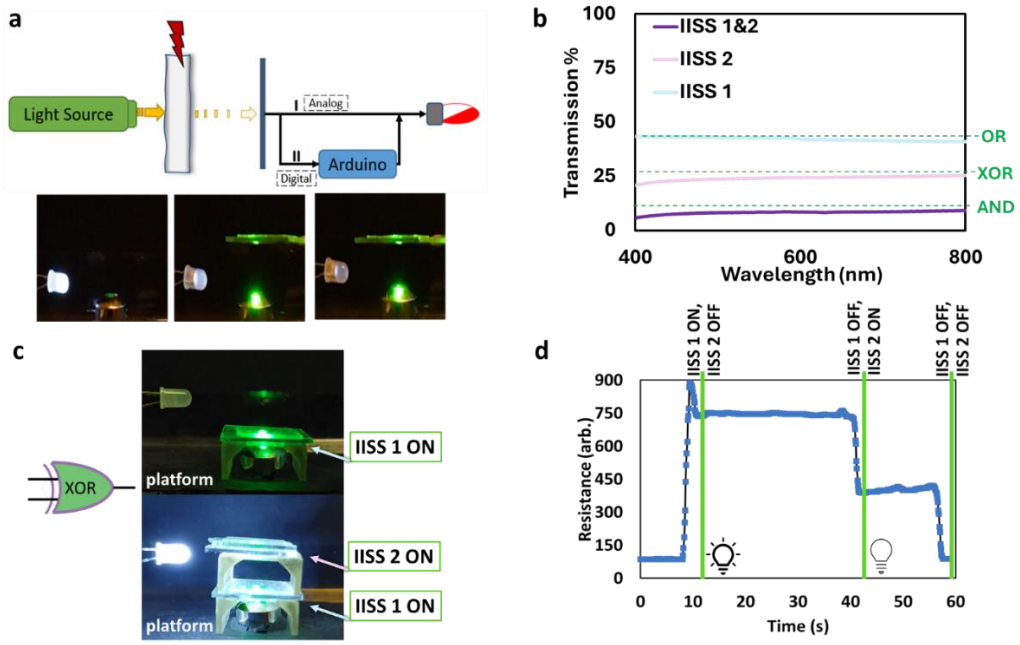

Supplementary Figure S13 (a) General schematic of constructed soft actuator device whereby light intensity (yellow) impinging on a photoresistor (dark-blue) is modulated by incursion of IIS – presupposed by sufficient analyte concentration (dark-red bolt) to the hydrogel (grey). (i) direct analog current to an LED or (ii) digital current modulated by a basic Arduino program that sets the threshold current value for the ON and OFF states of the LED leading to discrete, all-or-nothing switching of the LED in digital connection. In the IIS-XOR Gated Electronic System (c,d), IISS activation is discernible at all times, but through the co-modulation of the system as a whole, actuation is triggered autonomously but only when intended by the operator.